



**You have downloaded a document from**  
**RE-BUS**  
**repository of the University of Silesia in Katowice**

**Title:** Different route of hydroxide incorporation and thermal stability of new type of water clathrate : X-ray single crystal and Raman investigation

**Author:** Mateusz Dulski, Katarzyna M. Marzec, Joachim Kusz, Irina Galuskina, Katarzyna Majzner, Evgeny Galuskin

**Citation style:** Dulski Mateusz, Marzec Katarzyna M., Kusz Joachim, Galuskina Irina, Majzner Katarzyna, Galuskin Evgeny. (2017). Different route of hydroxide incorporation and thermal stability of new type of water clathrate : X-ray single crystal and Raman investigation. "Scientific Reports" (2017, Vol. 7, iss. 1, art. no. 9046), doi 10.1038/s41598-017-08152-1



Uznanie autorstwa - Licencja ta pozwala na kopiowanie, zmienianie, rozprowadzanie, przedstawianie i wykonywanie utworu jedynie pod warunkiem oznaczenia autorstwa.



UNIwersYTET ŚLĄSKI  
W KATOWICACH



Biblioteka  
Uniwersytetu Śląskiego



Ministerstwo Nauki  
i Szkolnictwa Wyższego

# SCIENTIFIC REPORTS

OPEN

## Different route of hydroxide incorporation and thermal stability of new type of water clathrate: X-ray single crystal and Raman investigation

Mateusz Dulski<sup>1,2</sup>, Katarzyna M. Marzec<sup>3,4</sup>, Joachim Kusz<sup>5</sup>, Irina Galuskina<sup>6</sup>, Katarzyna Majzner<sup>4,7</sup> & Evgeny Galuskin<sup>6</sup>

Chlormayenite  $\text{Ca}_{12}\text{Al}_{14}\text{O}_{32}[\text{Cl}_2]$  ( $\diamond$ -vacancy) is partially hydrated micro porous mineral with hydroxide groups situated at various crystallographic sites. There are few mechanisms describing its hydration. The first one assumes  $\text{Cl}^-$  substitution by  $\text{OH}^-$  at the center of the structural cages (*W*-site). The second one determines the converting a  $\text{TlO}_4$  tetrahedron to a  $\text{TlO}_3(\text{OH})_3$  octahedron due to the replacement of oxygen at the *O2* site by three OH-groups according to the scheme:  $(\text{O}^{2-} + \text{WCl}^-) \rightarrow 3 \times \text{O}^{2-}\text{OH}$ . The third mechanism, not considered so far in the case of zeolite-like minerals, includes the hydroxide incorporation in form of hydrogarnet defect due to the arrangement of tetrahedral  $(\text{OH})_4$  in vacant cages. This yields a strong hydrated phase containing even up to 35% of water more than in any currently known mineral applicable to Portland cement. Moreover, water molecules present in different structural cages are stable up to 355 K while dehydroxylation linked to the gradual loss of only 8% of  $\text{OH}^-$  groups according to  $3\text{O}^{2-}\text{OH}^- \rightarrow \text{O}^{2-} + \text{WOH}^- + \text{H}_2\text{O}$  occurs at temperature range from 355 K to 598 K.

The name mayenite was originally given to an isostructural mineral with a composition close to  $\text{Ca}_{12}\text{Al}_{14}\text{O}_{33}$  ( $\text{C}_{12}\text{A}_7$ ) discovered at the so-called *type locality*, Bellerberg volcano near Mayen, Eifel, Germany<sup>1</sup>. However, even this mineral name is used nowadays in various scientific disciplines such as chemistry, material sciences, and physics, it is not completely correct in relation to the mineralogy. A recent re-investigation studies of natural mayenite showed that (1) the composition of mayenite from the *type locality* is closer to  $\text{Ca}_{12}\text{Al}_{14}\text{O}_{32}\text{Cl}_2$ , and that (2) all samples from other occurrences are either fluorine or chlorine derivatives of  $\text{Ca}_{12}\text{Al}_{14}\text{O}_{32}[\text{O}](\text{C}_{12}\text{A}_7)^{2-5}$ . Thus, mayenite has been renamed to “chlormayenite” while the name “mayenite” was reserved for a potentially new mineral  $\text{Ca}_{12}\text{Al}_{14}\text{O}_{33}$ <sup>4</sup>.

Mayenite compounds can be applied as an ion or electron conductor<sup>6–10</sup>, catalyst in fuel processing<sup>11</sup>, or hydraulic active phase in cement<sup>12–14</sup> due to their chemical and physical properties such as conductivity, or the potential for water accumulation<sup>15–18</sup>. The mayenite features result from the zeolite-like framework  $\{\text{Al}_{14}\text{O}_{32}\}^{22-}$  enclosing six structural cages occupied by two Ca atoms, which leads to an excess of two positive charges<sup>19</sup>. The existence of 33<sup>rd</sup> extra-framework  $\text{O}^{2-}$  was postulated as statistically distributed over the six structural cages<sup>19</sup> and its site is a little bit shifted towards the cage wall<sup>20, 21</sup>. Recent studies of a synthetic fluoride<sup>22, 23</sup> or chlorine<sup>24</sup>

<sup>1</sup>Institute of Material Science, University of Silesia, 75 Pułku Piechoty 1a, 41-500, Chorzow, Poland. <sup>2</sup>Silesian Center for Education and Interdisciplinary Research, 75 Pułku Piechoty 1a, 41-500, Chorzow, Poland. <sup>3</sup>Center for Medical Genomics (OMICRON), Jagiellonian University, Kopernika 7C, 31-034, Krakow, Poland. <sup>4</sup>Jagiellonian Centre for Experimental Therapeutics (JCET), Jagiellonian University, Bobrzynskiego 14, 30-348, Krakow, Poland. <sup>5</sup>Institute of Physics, University of Silesia, Uniwersytecka 4, 40-007, Katowice, Poland. <sup>6</sup>Department of Geochemistry, Mineralogy and Petrography, Faculty of Earth Sciences, University of Silesia, Bedzinska 60, 41-200, Sosnowiec, Poland. <sup>7</sup>Faculty of Chemistry, Jagiellonian University, Ingardena 3, 30-060 Krakow, Poland. Correspondence and requests for materials should be addressed to M.D. (email: [mateusz.dulski@smcebi.edu.pl](mailto:mateusz.dulski@smcebi.edu.pl))

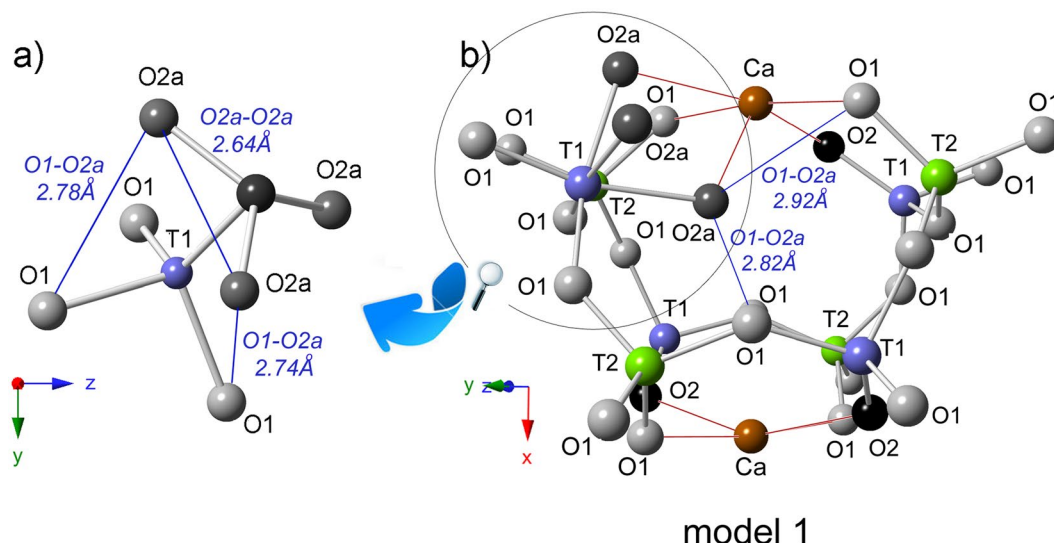


**Figure 1.** (a) Octahedral aluminum coordination at T1 and (b) potential acceptors for H-bond formation.

derivatives of  $C_{12}A_7$  have shown that 2  $F^-$  or 2  $Cl^-$  ions substitute the extra-framework,  $O^{2-}$  occupying the center of the structural cage<sup>25</sup>.

The key issue in order to characterize the synthetic mayenite and their natural counterparts is the analysis of hydration process. It is crucial in the development of new type of cement as well as in solving various geological problems. The process of water incorporation was previously reported due to the scheme:  $Ca_{12}Al_{14}O_{32}O + {}^8H_2O = Ca_{12}Al_{14}O_{32}(OH)_2$ , where two  $OH^-$  groups occupying the  $W$ -site are stable up to 1500 K<sup>26,27</sup>. However, temperatures associated with dehydration or dehydroxylation processes for these mineral phases have been not determined yet. Another mechanism of hydroxide incorporation is connected with the presence of the “unusual  $H_2O$  molecule” which occupies the empty structural cages according to the scheme:  $Ca_{12}Al_{14}O_{32}[\diamond_4(F,Cl)_2] + {}^8H_2O = Ca_{12}Al_{14}O_{32}[(H_2O)_4(F,Cl)_2]$ <sup>3,5</sup>. It has been shown that the molecular water is completely released from the mineral structure at a temperature range between 700–850 K.

This paper presents detailed studies of chlormayenite from Eifel with a simplified formula  $Ca_{12}Al_{13.5}Fe^{3+}_{0.5}O_{31.3}(OH)_{2.1}[\diamond_{4.7}Cl_{1.3}]$  as well as describes a various route of hydroxide incorporation into its crystal structure. The single crystal X-ray diffraction technique and Raman spectroscopy were applied to develop different models of hydroxylation. Structure stability under various temperatures were analyzed in detail based on *ex-situ* heated grains at 573 K, 773 K and 1073 K as well as *in-situ* one at the temperature range between 293 K and 873 K. Hence, the paper will provide a wide knowledge of the characterization of the mechanisms of hydroxide incorporation, H-bonding scheme and thermal stability of chlormayenite.

### X-ray diffraction and Raman spectroscopy data of natural chlormayenite

The chemical composition of a natural chlormayenite is expressed by  ${}^{x1}Ca_{12}{}^{T1}(Al_{7.54}Fe^{3+}_{0.46}){}^{T2}Al_6(O_1O_{24}O_{27.24}\diamond_{0.76})_{32}O_{2a}(OH)_{2.26}{}^W[\diamond_{4.75}Cl_{1.25}]$  with simplified formula:  $Ca_{12}Al_{14}O_{31.24}(OH)_{2.26}[\diamond_{4.75}Cl_{1.25}]$  and consists of end-members:  $Ca_{12}Al_{14}O_{32}Cl_2$  (62.5 mol.%) and  $Ca_{12}Al_{14}O_{30}(OH)_6$  (37.5 mol.%)<sup>2</sup>. X-ray outcomes translate directly to the chlormayenite framework which forms two  $T$ -aluminum sites  $\{T_{14}O_{32}\}$ . In the  $Ca_{12}Al_{14}O_{32}Cl_2$  end-member, the  $T2$ -site is four coordinated with the site symmetry  $-4$ , while the  $T1$  with site symmetry 3 is situated at the threefold axis.  $T1$ -aluminum tetrahedra shares only three bonds with O1 while the fourth apex is formed by O2 oxygen (Fig. 1). The crystal framework is terminated by O2 which is not shared with an adjacent tetrahedron. Here, only 1/3 of the cages are occupied by chlorine and this member may be subdivided into 21% of  $Cl^-$  containing at  $W$ -site and 42% of vacant  $W$  cages. The low values of atomic displacement for all tetrahedral framework sites indicates their very strong similarity independent of whether  $W$ -sites are occupied or vacant (data not shown)<sup>2</sup>. In turns, the  $Ca_{12}Al_{14}O_{30}(OH)_6$  end-member is characterized by octahedral T1 with O2 which may partially be replaced by three  $OH^-$  groups (O2a). After such structural change, three of the O2a ligands form an equilateral triangle (model 1 in Fig. 1a). Moreover, the short distance of 1.76 Å between O2a and W requires that the  $W$ -site must be vacant. All structural cages are filled by a pair of  $X = Ca$  atoms with site symmetry 2 coordinated by four O1 and two O2 sites. Two  $X$ -sites enclose a central cage of about 5 Å in a diameter. Bond lengths for chlormayenite summarized in Table 1. The different cages considered here have following characteristics (1) 4T1 and 4T2 tetrahedra with vacant  $W$  in the center (C1); (2) 4T1 and 4T2 tetrahedra with chlorine in the center (C2); (3) 3T1 tetrahedra, T1 octahedron, and 4T2 tetrahedra with vacant  $W$ -site (C3); (4) 4T1 and 4T2 tetrahedra with hydroxide in the center in which the adjacent  $X$ -sites are shifted towards the center of the cage due to size and charge of the anion (C4) (Fig. 2).

The potential acceptors of hydrogen bonds in C3 (O2a donor) are the adjacent O2a of the  $AlO_3OH_3$  octahedral with 2.64 Å bond distance (Fig. 1a). The two O1 sites defining the triangular face O2a-O1-O1 of the  $AlO_3OH_3$  octahedron are the second closest potential H-bond acceptors with a donor-acceptor (D-A) distances of 2.74 Å and 2.78 Å (Fig. 1a). Further potential acceptors are determined for O1 of adjacent  $T2O_4$  tetrahedra with D-A

		100 K [2]	573 K	773 K	1073 K
<b>Distance [Å]</b>					
Ca1	O1 × 2	2.386 (4)	2.3821 (3)	2.3743 (4)	2.3738 (4)
	O1 × 2	2.496 (4)	2.4924 (5)	2.5027 (11)	2.5042 (15)
	O2 × 2	2.416 (4)	2.4138 (3)	2.4198 (4)	2.4142 (5)
	O2a* × 2	2.256 (4)	2.254 (4)	—	—
	O2a* × 2	2.485 (5)	2.476 (4)	—	—
	<sup>W</sup> Cl	2.854 (2)	2.8508 (4)	2.8508 (12)	2.8386 (17)
Ca2	O1 × 2		2.3855 (11)	2.3829 (11)	2.3826 (17)
	O1 × 2		2.786 (11)	2.845 (8)	2.837 (14)
	O2 × 2		2.3584 (12)	2.3600 (7)	2.3564 (11)
	<sup>W</sup> OH		—	2.451 (9)	2.450 (15)
T1	O1 × 3	1.790 (4)	1.7864 (3)	1.7842 (4)	1.7790 (5)
	O2*	1.714 (8)	1.7130 (7)	1.7333 (8)	1.7298 (8)
	O2a* × 3	2.098 (5)	2.099 (4)	—	—
T2	O1 × 4	1.746 (4)	1.7440 (3)	1.7465 (4)	1.7422 (4)

**Table 1.** Selected interatomic distances of untreated chlormayenite<sup>2</sup> and annealed crystals at 573 K and 773 K and 1073 K. \*Either O2 or 3 × O2a are occupied.

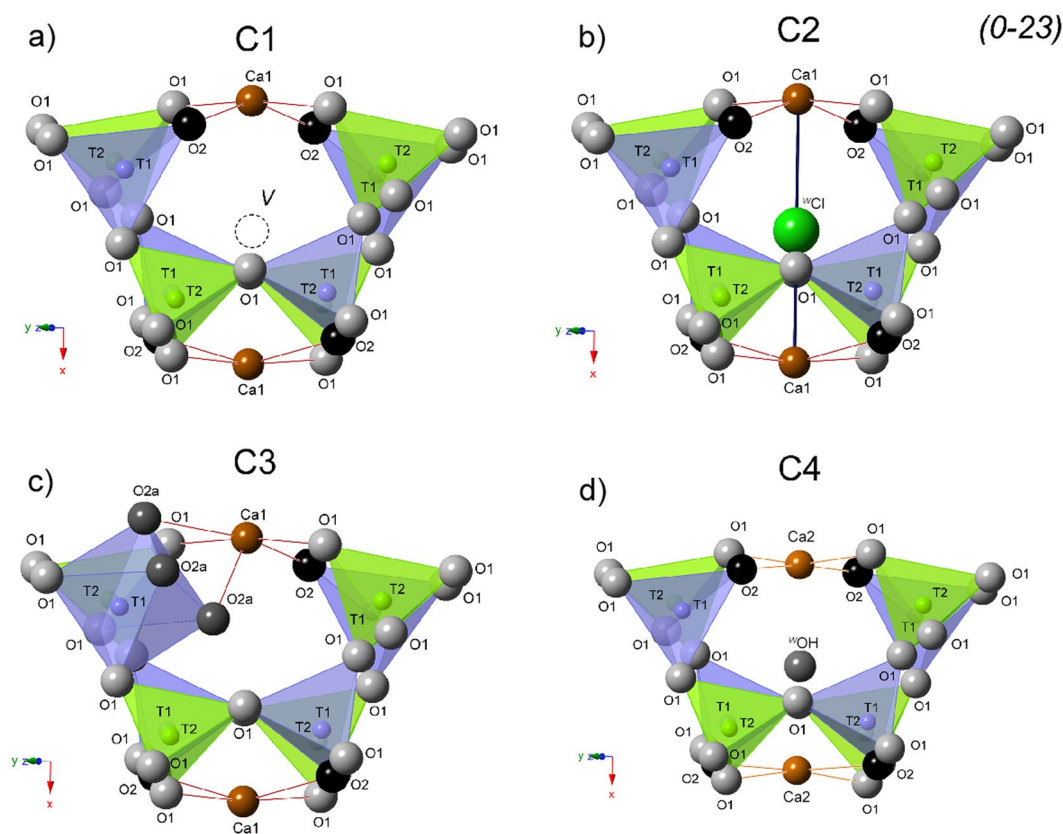


**Figure 2.** Four different cages of chlormayenite, inclusive extra-framework ions projected onto (0-23). The cage (a) C1 is unfilled, (b) C2 is filled by <sup>W</sup>Cl<sup>-</sup> (green sphere), (c) C3 in which one of the tetrahedral sites T1 (violet) is hydroxylated, whereby <sup>O2a</sup>3OH<sup>-</sup> replace one oxygen at O2 (black spheres). The tetrahedral site T2 (dark blue) connects four times to O1 (dark gray spheres). (d) Cage C4 with OH group (gray sphere) situated at the W-site which drags the adjacent Ca1 (brown spheres) into the cage center (Ca2).

distances of 2.82 Å and another O1 across the cage with a D-A distance of 2.92 Å (model 1 in Figs 1b and 3a). It turns, X-ray structural refinement of C4 indicated D-A distance between <sup>W</sup>OH donor and O1 or O2 acceptors, respectively as 3.26 Å and 3.29 Å (model 2 in Fig. 3b). Furthermore, an indicator of hydrogen bonds seems also to be the bond valence calculations for the potential acceptor atoms<sup>28,29</sup>. Here, the calculate valence deficit of around



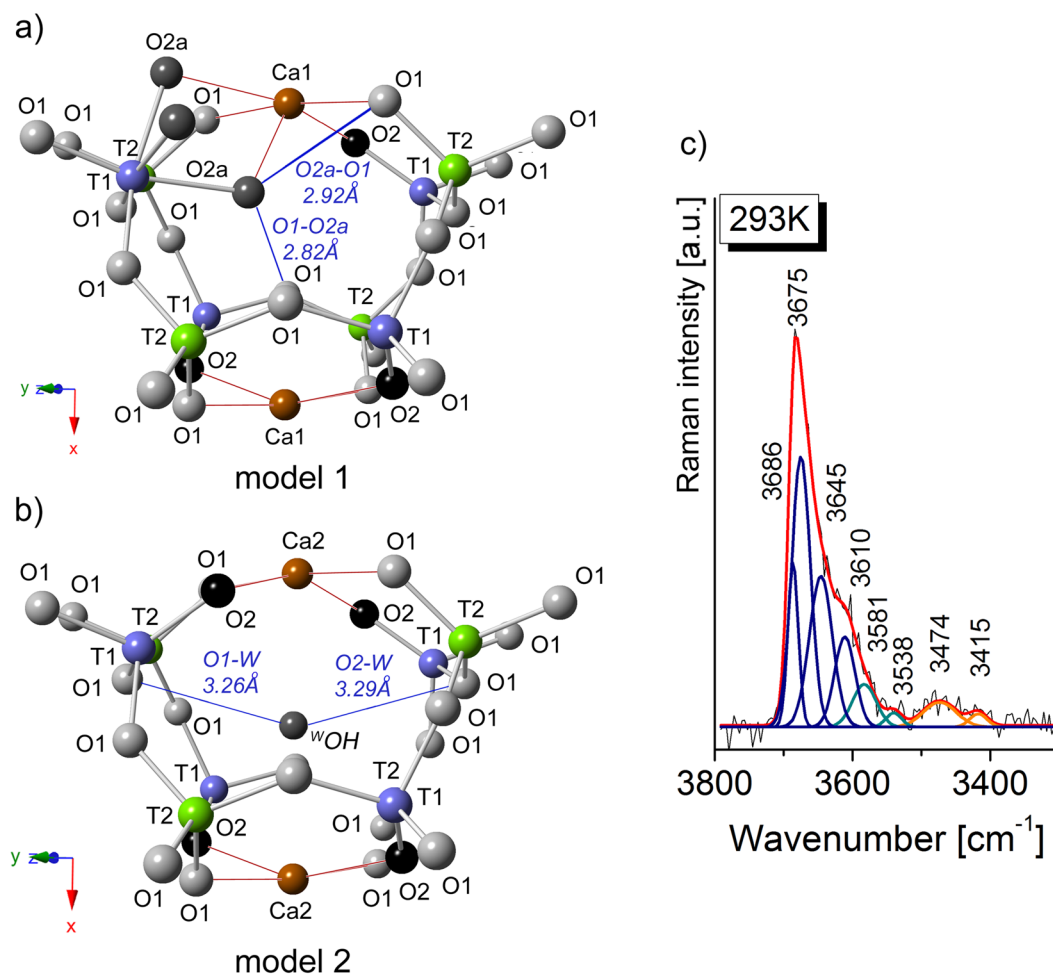


**Figure 3.** (a) Raman spectrum in the hydroxyl stretching region. (b,c) Two models of hydroxide group distribution observed for the structural cages C3 and C4. The images were projected onto (0–23) in which O1, O2 or O2a atoms are potential acceptors for hydrogen bonds.

0.08 vu (valence units) for O1 slightly higher than the deficit of the OH-groups at O2a (0.02 vu) suggests that none of these oxygen sites are appropriate as an acceptor of a hydrogen bond in case of cage C3<sup>28</sup>. On the other hand, the bond valence increase of ca. 0.23 vu for acceptor oxygen with OH...O distance through ca. 3.20 Å<sup>29</sup>. It suggests that hydroxyl groups at W-site like in C4 makes the potential H-bond with acceptors at O1 ( $d_{\text{OH}\cdots\text{O}} \approx 3.26$  Å) and at O2 ( $d_{\text{OH}\cdots\text{O}} \approx 3.29$  Å). What is more, the O1 acceptor due to shorter  $d_{\text{OH}\cdots\text{O}}$  distance may form a stronger H-bond than oxygen in O2 site. However, the real molecular structure may differ from the model structure and bond valence calculations have to be treated with considerable caution. Hence, relying only on such approach, it is difficult to predict real configuration of the hydroxyl group orientation and the most favorable proton arrangement in particular O...O direction.

Therefore, to solve the problem of hydroxide groups in chlormayenite crystal structure the theoretical and experimental Raman studies have been performed. Theoretical approach developed first by Nakamoto and corrected further by Libowitzky has a form of the equation which describes the dependence between the hydroxyl Raman band position and the O...O bond distance ( $d_{\text{O}\cdots\text{O}}$ )<sup>30,31</sup>. Nakamoto diagram predicts an occurrence of Raman bands assigned to the OH modes in the region of 3660–2070 cm<sup>-1</sup> when O...O distances varied in the range of 2.50–3.20 Å<sup>31</sup>. On the other hand, Libowitzky relation reports that the  $d_{\text{O}\cdots\text{O}} = 2.44$ –3.50 Å are linked to Raman bands in wide wavenumbers range from 3582 to 1758 cm<sup>-1</sup><sup>30</sup>.

The fitting procedures performed for the hydroxyl region on the chlormayenite grains reveals a different type of vibrations which might be separated into three spectral regions of (1) 3750–3580 cm<sup>-1</sup>, (2) 3580–3500 cm<sup>-1</sup> and (3) 3500–3300 cm<sup>-1</sup> (Fig. 3c). In the region (1) the bands appear at 3686, 3675, 3645 and 3610 cm<sup>-1</sup>, however, their nature is not quite clear. According to Nakamoto diagram, these bands might correspond to the  $d_{\text{O}\cdots\text{O}}$  distance equal to 3.20, 3.10 and 3.00 Å suggesting the OH group presence within cage C4. However, Libowitzky equation showed, the  $d_{\text{O}\cdots\text{O}}$  distance is not fully conclusive and points to an atypical hydroxyl group arrangements. Moreover, the presence of O2a oxygen as a potential proton acceptor should lead to the formation of structural defects, which are statically or dynamically disordered in the mayenite structure. This issue is much more complicated and will be discussed in detail further on. The bands of the region (2) arise probably from the

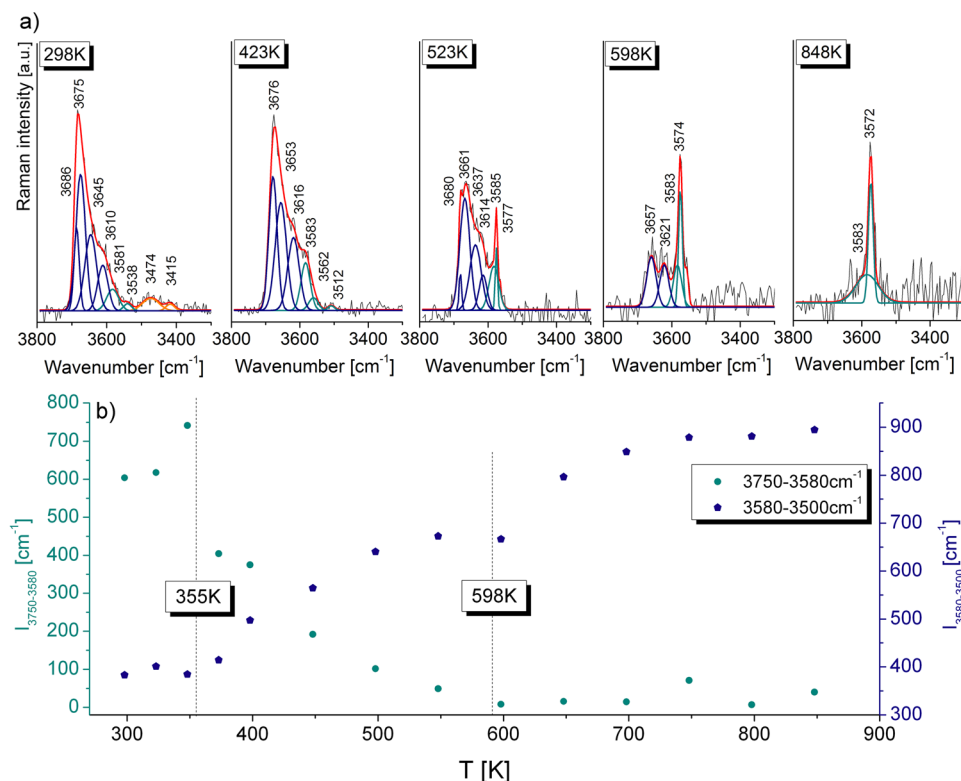


**Figure 4.** (a) The example temperature-dependent Raman spectra of chlormayenite in the hydroxyl stretching region. (b) The alteration of integral intensity values as a function of temperature in two regions: 3750–3580  $\text{cm}^{-1}$  and 3580–3500  $\text{cm}^{-1}$ .

vibration of hydroxyl group occupied *W*-site of cage C4. It is worth to note that Nakamoto diagram does not work here well while Libowitzky formula predicts  $d_{\text{O}^2\text{a}-\text{O}}$  bond distance close to 3.10 Å and 3.00 Å. It corresponds to bands with the maximum at 3581 and 3538  $\text{cm}^{-1}$  (model 2 in Fig. 3b) and correlates to interpretations for synthetic mayenite<sup>32,33</sup>. In turns, bands with relatively low intensity observed in the region (3) might originate from an  $\text{O}2\text{a}-\text{O}1$  bond distance with length equal to 2.92 Å, and 2.82 Å as can be predicted on the base of theoretical XRD data for cage C3.

### X-ray diffraction and Raman spectroscopy data of heat treated chlormayenite crystals

The structural studies and electron microprobe analysis (EMPA) were carried out on individual grains and gave the opportunity to obtain their general crystal chemical formulas:

- 573 K:

$\text{X}^1\text{Ca}_{11.4}\text{X}^2\text{Ca}_{0.6}\text{Tl}(\text{Al}_{7.52}\text{Fe}^{3+}_{0.48})\text{Tl}_2\text{Al}_6(\text{O}^1\text{O}_{24}\text{O}^2\text{O}_{7.36}\text{O}^{0.64})_{32}\text{O}^{2\text{a}}(\text{OH})_{1.92}\text{W}[\text{Cl}^*_{4.59}\text{Cl}^*_{1.41}]$ , where  $\text{Cl}^* \approx 1.11\text{Cl} + 0.3\text{OH}$  with simplified formula:  $\text{Ca}_{12}\text{Al}_{14}\text{O}_{31.36}(\text{OH})_{1.92}[\text{Cl}^*_{4.59}\text{Cl}^*_{1.11}(\text{OH})_{0.30}]$

- 773 K:

$\text{X}^1\text{Ca}_{10.24}\text{X}^2\text{Ca}_{1.76}\text{Tl}(\text{Al}_{7.52}\text{Fe}^{3+}_{0.48})\text{Tl}_2\text{Al}_6(\text{O}^1\text{O}_{24}\text{O}^2\text{O}_8)_{32}[\text{Cl}^*_{3.93}\text{Cl}^*_{1.19}(\text{OH})_{0.88}]$  with simplified formula:  $\text{Ca}_{12}\text{Al}_{14}\text{O}_{32}[\text{Cl}^*_{3.93}\text{Cl}^*_{1.19}(\text{OH})_{0.88}]$

- 1073 K:

$\text{X}^1\text{Ca}_{10.36}\text{X}^2\text{Ca}_{1.64}\text{Tl}(\text{Al}_{7.52}\text{Fe}^{3+}_{0.48})\text{Tl}_2\text{Al}_6(\text{O}^1\text{O}_{24}\text{O}^2\text{O}_8)_{32}[\text{Cl}^*_{3.88}\text{Cl}^*_{1.3}(\text{OH})_{0.82}]$  with simplified formula:  $\text{Ca}_{12}\text{Al}_{14}\text{O}_{32}[\text{Cl}^*_{3.88}\text{Cl}^*_{1.3}(\text{OH})_{0.82}]$

The small differences in the cation composition with relation to the average composition of EMPA:  $\text{Ca}_{12}\text{Al}_{13.5}\text{Fe}^{3+}_{0.5}\text{O}_{31.3}(\text{OH})_{2.1}[\text{Cl}^*_{4.7}\text{Cl}^*_{1.3}]$  can be explained by the different chlormayenite grains which were taken into consideration through the studies. However, the chemical composition of various grains is slightly different from each other and does not affect the further analysis. Noticeable differences are appearing during the annealing process up to 573 K, 773 K and 1073 K. Annealing at 573 K decreases the number of OH groups at O2a from originally 10%<sup>2</sup> to about 8% wherein the occupancy at the *W*-site slightly increases (Table S1 in supplementary file). Those changes may be described to the scheme:  $\text{O}^{2\text{a}}3\text{OH}^- + \text{O}^{2\text{a}}\text{O}^{2-} + \text{W}^-\text{OH}^- + \text{H}_2\text{O}$  and the data are in agreement with the model. In addition, the refined crystal structure of sample annealed at 573 K points to the splitting of Ca which results in occupancies of 0.973(2) for Ca1 and 0.027(2) for Ca2. However, the small electron density of OH<sup>-</sup> at *W*-site is overlapping with the one of Cl<sup>-</sup> and cannot be refined separately (Table S1 in supplementary file). After crystal annealing at 773 K and 1073 K, OH groups originally located at the O2a site are no longer detected (Table S1 in supplementary file) and Tl converts to tetrahedral coordination. In addition, the refined

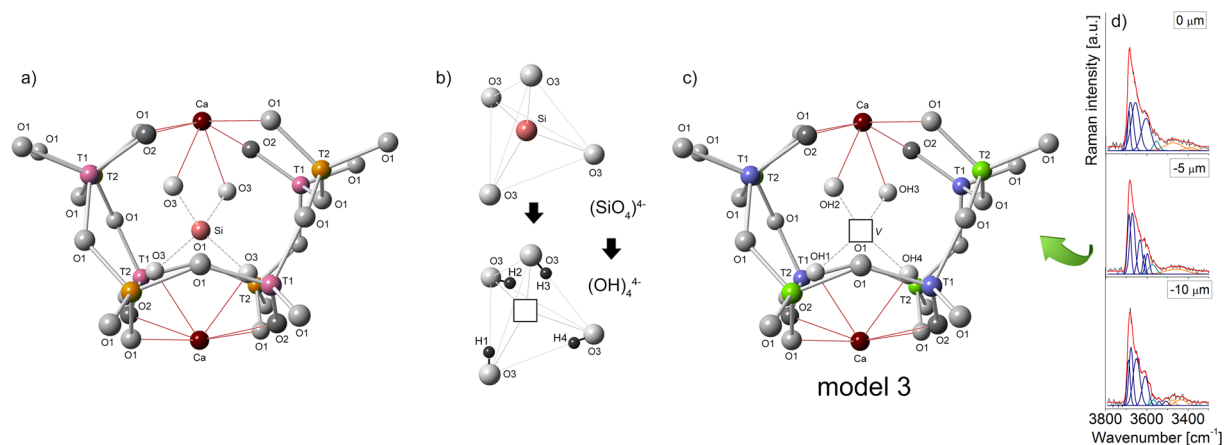


**Figure 5.** (a) Atom arrangement in a grossular-like structure where T1 and T2 are ascribed to the position of silicon, (b) schema of the hydrogarnet substitution:  $(\text{OH})_4 \rightarrow \text{SiO}_4$  where hydrogens occupied an outer position within the tetrahedron between two unshared system edges (modified from ref. 37). (c) Atom arrangement assumed in mayenite-like structure with selected hydrogarnet defect where T1 and T2 are the silicon position. (d) Raman spectra of chlormayenite crystal measured in depth profile and fitted by Voigt function.

structure of crystal annealed at 773 K shows an increase of the electron density at *W*-site and 0.2 Cl<sup>-</sup> at *W*-site converges to ca. 0.14 additional OH<sup>-</sup>. This central OH attracts adjacent Ca, and leads to split the calcium positions into *Ca1* and *Ca2* (due to OH). Since a considerable amount of OH<sup>-</sup> moving to *W*-site at 773 K, the occupancy factor of OH<sup>-</sup> has been constrained to the occupancy of displaced *Ca2* (0.147(6)) while the occupancy of Cl<sup>-</sup> at *W*-site (0.199(3)) were refined as detached from OH<sup>-</sup> (Table S1 in supplementary file). The data set of the measurement at 1073 K has been refined identically to the measurement carried out at 773 K. For all refinements, the anisotropic displacement parameters for OH<sup>-</sup> and Cl<sup>-</sup> at *W*-site have been set equally (Tables S2–S3 in supplementary file). It is worth to add that the bond distances between *Ca1*-O are practically unaffected by temperature (Table 1) while for the average *Ca2*-O bond distance, only an individual *Ca2*-O1 value increases to around 2.84 Å after annealing at 773 K and 1073 K (Table 1). Additionally, similar like for unheated crystal, the presence of hydroxyl groups at *W*-site at all of the annealed samples points to the potential H-bond acceptors at O1 ( $d_{\text{OH}\cdots\text{O}} \approx 3.26$  Å) and at O2 ( $d_{\text{OH}\cdots\text{O}} \approx 3.29$  Å). It should as well be noticed that the shift of *Ca1* to *Ca2* results in a higher bond valence deficit for the O1 (0.230 vu) sites than for O2 (0.226 vu) at the OH-populated cage wall. In consequence, the proton-acceptor oxygen in O1 site seems to be formed a stronger H-bond than oxygen in O2 site.

On the Raman spectrum of unheated crystal, weak bands at 3581 cm<sup>-1</sup> and 3538 cm<sup>-1</sup> resulted from the presence of single hydroxyl group occupied the central part of the C4 cage. Further, bands at 3474 and 3415 cm<sup>-1</sup> reflect a process of partial hydration in which a small number of T1 aluminum changes its coordination from tetrahedral to octahedral as a result of further protonated oxygen by the scheme:  $\text{O}^{2-} + \text{WCl}(\text{F})^- \rightarrow \text{O}^{2+}3\text{OH}^-$ . Moreover, to determine the dehydroxylation temperature and analyze the thermal stability of  $\text{O}^{2+}\text{OH}$  chlormayenite unit, the temperature-dependent *in-situ* Raman measurements on one single crystal were performed (Fig. 4). The thermal experiment has shown the change of the integral intensity values in two spectral hydroxyl regions which were associated with a reorganization of OH within C3. The intensities of the Raman bands in regions (1) 3750–3580 cm<sup>-1</sup> and (3) 3500–3300 cm<sup>-1</sup> decreased while for bands in the region (2) 3580–3500 cm<sup>-1</sup> increased with rising temperature. Moreover, the disappearance of the band centered at 3686 cm<sup>-1</sup> suggests vanishing of the absorbed water from a mineral surface while reorganization of OH groups starts above 355 K and ends at about 598 K (Fig. 4a,b).

## Discussion

Recently published papers highlighted the existence of two routes of hydroxide incorporation into the chlormayenite crystal structure. The most energetically favorable mechanisms assumed replacement of one oxygen positioned at the O2 site by three OH<sup>-</sup> groups and converting of a  $\text{TlO}_4$  tetrahedron to a  $\text{TlO}_3(\text{OH})_3$  octahedron (model 1 in Figs 1 and 3a) as well as substituting of chlorine atom by one OH<sup>-</sup> ion into a central *W*-site (model 2 in Fig. 3b). The presence of  $\text{O}^{2+}\text{OH}$  groups distinguishes two O–O distances:  $\text{O}^{2+}\text{O}1 = 2.92$  Å,  $\text{O}^{2+}\text{O}1 = 2.82$  Å which due to Libowitzky correlation ought to be associated with medium strength hydrogen bonds<sup>30</sup>. In turns, the hydroxyl units occupied the *W*-site and give rise to the formation of a weak H-bonds by the location of hydrogen acceptors at O1 ( $d_{\text{O}\cdots\text{O}} \approx 3.26$  Å) and at O2 ( $d_{\text{O}\cdots\text{O}} \approx 3.29$  Å) with a bond-valence sum close to 1.73 vu for O1 and O2 oxygen. The theoretical models are referring to Raman spectrum in the 3600–3200 cm<sup>-1</sup> range whereas the nature of bands with strong intensity above 3600 cm<sup>-1</sup> is still not resolved and remains a subject of intense discussion.

In order to solve the origin of undefined chlormayenite bands on Raman spectrum, it is necessary to consider two concepts: (1) the process of hydroxide incorporation into the structure of garnets<sup>34–36</sup> and (2) electrostatic interaction between a proton and cations (including other protons) due to the formation of hydrogarnet defects (Fig. 5a). Hydrogrossular<sup>37–39</sup>, andradite<sup>40</sup> and other garnets belong to minerals forming at anomaly low

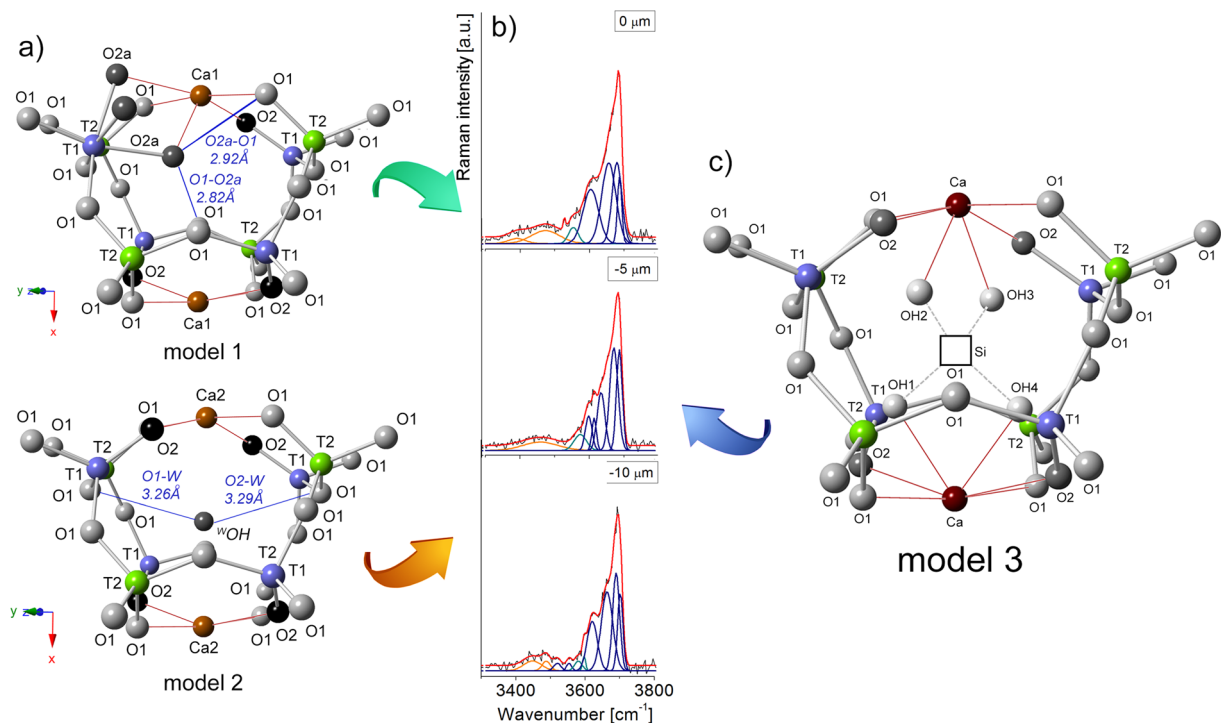


**Figure 6.** (a) Theoretical models of chlormayenite cages based on the diffraction data, (b) Raman spectra in hydroxyl stretching region measured in depth profile, (c) hydroxyl group arrangement into the structure of chlormayenite. The images were projected onto (0–23) in which O1, O2 or O2a atoms are highlighted as potential acceptors for hydrogen bonds.

pressures (~ few bars) and temperature of 1000–1350 K while the process of water incorporating into their structure provides formation of hydrogarnet defects in which four O atoms around a silicon vacancy are terminated by hydroxyl groups<sup>34,35,38</sup> (Fig. 5b). A similar condition is crucial to form synthetic Sr-hydrogarnet with a structure closely related to mayenite<sup>36</sup>. However, the degree of hydration strictly depends on the number of OH<sup>−</sup> ions, the length of shared or unshared polyhedral edges<sup>41</sup>. The high temperature and low pressure conditions are linked to the formation, structurally and chemically similar to garnets, porous mayenite-type phases with the possibility of storing inside the cage, haloids (e.g. chlorine, fluorine), or oxygen according to general pattern  $\text{Ca}_{12}\text{Al}_{14}\text{O}_{28}\text{O}_4[\text{F}_4(\text{F},\text{Cl})_2]$  (Fig. 5c). In such minerals, the chlorine or fluorine ions distributed in the vacancies, form so-called mayenite defects<sup>42</sup>. Similar conditions of a mayenite-type mineral formation, relative to garnets might favor the emergence of hydrogarnet defects (Fig. 5b and c). However, their appearance will strictly depend on insufficiently high haloid activity, and high abundance of water in the environment. In addition, such groups will not only be linked to the surface but will be distributed in the whole structure (Fig. 5d). Therefore, the water capacity of the mayenite-type structure becomes even a few times higher than previously described in literature<sup>2</sup>.

To shed more light on chlormayenite spectrum in region (1), the obligatory is to look more precisely into the data for garnets. It is due to the correlation between position of hydroxide within polyhedral sites with bands centered between 3700–3500 cm<sup>−1</sup>. Literature reports that the tetrahedral hydrogarnet substitution in hydrogrossular gives rise to overlapping bands centered around 3660 and 3600 cm<sup>−1</sup> wherein the hydroxide content linearly correlates with the intensity of hydroxyl bands<sup>43</sup>. More detailed studies revealed that band around 3660 cm<sup>−1</sup> originates from a presence of very weak hydrogen bond scheme within the (OH)<sub>4</sub> tetrahedron<sup>34</sup>. Here, one can look more closely on the electrostatic interaction between atoms to explain the origin of the band. The size of this subunit is smaller in relation to typical tetrahedron implying appearance of an electrostatic interaction. As a result, the repulsive force between proton and cations including other protons of OH groups starts to have a stronger influence than attraction force typically considered in a crystalline structure. As a result, such Raman band is shifted towards higher wavenumber. Similar band assignment was also found for a natural and synthetic hydroandradite. However, in the case of these minerals, a shift of hydroxyl bands towards lower wavenumber (3610 and 3560 cm<sup>−1</sup>) might be assigned to the greater average of tetrahedral cation-cation distance within (OH)<sub>4</sub> group, what implies a decrease of repulsive force and increase the share of attraction ones<sup>44</sup>. Finally, detailed studies for non-cubic garnet such as uvarovite-grossular highlighted that Raman bands observed at 3652, 3640 and 3602 cm<sup>−1</sup> originate from vacancies on octahedral or dodecahedral cation sites<sup>45</sup>. Thus, the great variability and complexity of the chlormayenite spectrum prove that hydrogarnet substitution probably plays an essential role during water incorporation (model 3 in Fig. 6). Moreover, it may be a key process in clarifying a route of a hydration and help in a description of hydrogen storage mechanism in nominally anhydrous or low hydrous mayenite-type structure minerals. Hence, description of water incorporation will be the first step to expand physicochemical properties of mayenite-type phases, provides unique information about their formation, and finally



helps to develop the hypothesis of formation a strongly hydrated garnet-type structure mineral, katoite. This phase is typical for mayenite cement<sup>46</sup> and gives an opportunity to improve features of building materials, especially sulfur corrosion resistance<sup>47</sup>. It is worth to note here that the hydrogarnet defect leads to the appearance of repulsive force between protons within the (OH)<sub>4</sub> unit or proton and calcium acting the only way to explain the problem of Raman bands in the 3800–3600 cm<sup>-1</sup> region.

Raman experiment and X-ray diffraction data shed a new light on the temperature stability of <sup>02a</sup>OH, and (OH)<sub>4</sub> with relation to <sup>w</sup>OH groups. The temperature-dependent *in-situ* Raman experiment shows that position of bands from regions (1) and (2) are slightly red shifted (Fig. 4a) while the intensity of bands from region (1) is decreasing with temperature rise. The band near 3682 cm<sup>-1</sup> disappears at 355 K, supports its assignment to the OH<sup>-</sup> group vibration of the surface water (Fig. 4b). Moreover, *in-situ* Raman analysis shows that two bands of region (3) arising from OH vibration typically occurs in the octahedral aluminum coordination which disappears at around 355 K as an effect of removal of <sup>02a</sup>OH moieties. These results confirm a very high instability of AlO<sub>3</sub>(OH)<sub>3</sub> units and provide proof of the transformation of structural subunits from octahedral to tetrahedral coordination (Fig. 4). More detailed *ex-situ* XRD and *in-situ* Raman experiments imply that aluminum tetrahedra above 355 K stayed intact without any trace of structural transformation. At the temperature of ~430 K, the most intense bands associated with hydrogarnet substitution are shifted towards higher wavenumber due to hydroxide mobility and weakening of the hydrogen interaction within the (OH)<sub>4</sub> groups. Similar outcomes were previously reported for hydrogrossular or Sr-hydrogarnet where hydroxyl group was stable up to 573 K<sup>48, 49</sup> or 673 K<sup>36</sup>. It turned out that a strong diffusivity of hydroxyl moieties might be responsible for a complete disappearance of characteristic chlormayenite bands at temperatures above 598 K. At the same time, temperature-dependent Raman data were correlated with an increase of band intensity from the region (2) according to the dehydroxylation scheme as Ca<sub>12</sub>Al<sub>13.5</sub>Fe<sup>3+</sup><sub>0.5</sub>O<sub>31.3</sub>(OH)<sub>2.1</sub>[ $\blacklozenge_{4.7}$ Cl<sub>1.3</sub>] → Ca<sub>12</sub>Al<sub>13.5</sub>Fe<sup>3+</sup><sub>0.5</sub>O<sub>32</sub>[ $\blacklozenge_{4.7}$ Cl<sub>1.3</sub>(OH)<sub>0.7</sub>] + <sup>g0.7</sup>H<sub>2</sub>O, where some of OH groups are moving to the center of the structural cage balancing their charge. According to the literature, the OH group located in a central position formed weak hydrogen bonds which are stable even up to 1500 K<sup>2</sup>.

## Methods

The chemical composition was measured using a CAMECA SX100 electron microprobe operating in wavelength-dispersive spectrometry mode at 15 kV, 10–20 nA and using natural standards (Full description of the methodology is summarized in ref. 2). The single-crystal X-ray data were obtained using SuperNova Dual diffractometer with a mirror monochromator (MoK $\alpha$ , 0.71073 Å) and Atlas CCD detector. The structure was solved by direct methods, with subsequent analyses of difference-Fourier maps, and refined with neutral atom scattering factors using SHELX97<sup>50</sup>. Experimental details for untreated and annealed crystals summarized in supplementary file in Table S3. The Raman experiment was performed using WITec confocal CRM Alpha 300 Raman microscope at excitation laser line  $\lambda$  = 488 nm and CCD detector. The spectra were collected in the range between 4000–120 cm<sup>-1</sup> with the spectral resolution of 3 cm<sup>-1</sup> and integration time, 0.3 s for a single spectrum.

## References

- Hentschel, G. Mayenit, 12CaO·7Al<sub>2</sub>O<sub>3</sub>, und brownmillerit, 2CaO·(Al,Fe)<sub>2</sub>O<sub>3</sub>, zwei neue minerale in den kalksteinschlüssen der lava des Ettringer Bellerberges. *Neues Jahrb. Für Mineral. Monatshefte* 22–29 (1964).
- Galuskin, E. V. *et al.* A reinvestigation of mayenite from the type locality, the Ettringer Bellerberg volcano near Mayen, Eifel district, Germany. *Mineral. Mag.* **76**, 707–716 (2012).
- Galuskin, E. V. *et al.* Mayenite supergroup, part III: Fluormayenite, Ca<sub>12</sub>Al<sub>14</sub>O<sub>32</sub>[ $\blacklozenge_{4.7}$ F<sub>2</sub>], and fluorkyuygenite, Ca<sub>12</sub>Al<sub>14</sub>O<sub>32</sub>[(H<sub>2</sub>O)<sub>4</sub>F<sub>2</sub>], two new minerals from pyrometamorphic rocks of the Hatrurim Complex, South Levant. *Eur. J. Mineral.* **27**, 123–136 (2015).
- Galuskin, E. V. *et al.* Mayenite supergroup, part II: Chlorkyuygenite from Upper Chegem, Northern Caucasus, Kabardino-Balkaria, Russia, a new microporous mineral with ‘zeolitic’ H<sub>2</sub>O. *Eur. J. Mineral.* **27**, 113–122 (2015).
- Gfeller, F. *et al.* Mayenite supergroup, part IV: Crystal structure and Raman investigation of Al-free eltybyuinite from the Shadil-Khokh volcano, Kel’ Plateau, Southern Ossetia, Russia. *Eur. J. Mineral.* **27**, 137–143 (2015).
- Palacios, L. *et al.* Crystal structures and *in-situ* formation study of mayenite electrides. *Inorg. Chem.* **46**, 4167–4176 (2007).
- Hayashi, K., Matsuishi, S., Kamiya, T., Hirano, M. & Hosono, H. Light-induced conversion of an insulating refractory oxide into a persistent electronic conductor. *Nature* **419**, 462–465 (2002).
- Lacerda, M., Irvine, J. T. S., Glasser, F. P. & West, A. R. High oxide ion conductivity in Ca<sub>12</sub>Al<sub>14</sub>O<sub>33</sub>. *Nature* **332**, 525–526 (1988).
- Kim, S. W. *et al.* Metallic State in a Lime–Alumina Compound with Nanoporous Structure. *Nano Lett.* **7**, 1138–1143 (2007).
- Sushko, P. V., Shluger, A. L., Hayashi, K., Hirano, M. & Hosono, H. Role of hydrogen atoms in the photoinduced formation of stable electron centers in H-doped 12CaO·7Al<sub>2</sub>O<sub>3</sub>. *Phys. Rev. B* **73**, 045120 (2006).
- Li, C., Hirabayashi, D. & Suzuki, K. A crucial role of O<sup>2-</sup> and O<sub>2</sub><sup>2-</sup> on mayenite structure for biomass tar steam reforming over Ni/Ca<sub>12</sub>Al<sub>14</sub>O<sub>33</sub>. *Appl. Catal. B Environ.* (2009).
- Nurse, R. W. Phase Equilibria and Constitution of Portland Cement Clinker. in **1**, 32–33 (U. S. Department of Commerce. National Bureau of Standards, 1960).
- Roy, D. M. & Roy, R. Chemistry of Cement. in **43**, 307 (U. S. Department of Commerce. National Bureau of Standards, 1960).
- Zhen, G. *et al.* Hydration process of the aluminate 12CaO·7Al<sub>2</sub>O<sub>3</sub>-assisted Portland cement-based solidification/stabilization of sewage sludge. *Constr. Build. Mater. Complete*, 675–681 (2012).
- Medvedeva, J. E. & Freeman, A. J. Combining high conductivity with complete optical transparency: A band structure approach. *EPL Europhys. Lett.* **69**, 583 (2005).
- Medvedeva, J. E. & Freeman, A. J. Hopping versus bulk conductivity in transparent oxides: 12CaO·7Al<sub>2</sub>O<sub>3</sub>. *Appl. Phys. Lett.* **85**, 955–957 (2004).
- Strandbakke, R., Kongshaug, C., Haugsrud, R. & Norby, T. High-Temperature Hydration and Conductivity of Mayenite, Ca<sub>12</sub>Al<sub>14</sub>O<sub>33</sub>. *J. Phys. Chem. C* **113**, 8938–8944 (2009).
- Tsvetkov, D. S., Steparuk, A. S. & Zuev, A. Y. Defect structure and related properties of mayenite Ca<sub>12</sub>Al<sub>14</sub>O<sub>33</sub>. *Solid State Ion.* **276**, 142–148 (2015).
- Büsem, W. & Eitel, A. Die Struktur des Pentacalciumtrialuminats. *Z. Für Krist. - Cryst. Mater.* **95**, 175–188 (1936).
- Sakakura, T. *et al.* Determination of the local structure of a cage with an oxygen ion in Ca<sub>12</sub>Al<sub>14</sub>O<sub>33</sub>. *Acta Crystallogr. B* **67**, 193–204 (2011).
- Nomura, T. *et al.* Anion Incorporation-induced Cage Deformation in 12CaO·7Al<sub>2</sub>O<sub>3</sub> Crystal. *Chem. Lett.* **36**, 902–903 (2007).
- Williams, P. P. Crystal Structure of a Fluoride Derivative of 12CaO·7Al<sub>2</sub>O<sub>3</sub>. *J. Am. Ceram. Soc.* **51**, 531–531 (1968).
- Williams, P. P. Refinement of the structure of 11CaO·7Al<sub>2</sub>O<sub>3</sub>·CaF<sub>2</sub>. *Acta Crystallogr. B* **29**, 1550–1551 (1973).

24. Iwata, T., Haniuda, M. & Fukuda, K. Crystal structure of  $\text{Ca}_{12}\text{Al}_{14}\text{O}_{32}\text{Cl}_2$  and luminescence properties of  $\text{Ca}_{12}\text{Al}_{14}\text{O}_{32}\text{Cl}_2\text{:Eu}^{2+}$ . *J. Solid State Chem* (2008).
25. Boysen, H. *et al.* Structures and properties of variously doped Mayenite investigated by neutron and synchrotron powder diffraction. *Z. Krist. Suppl.* **2009**, 323–328 (2009).
26. Hayashi, K., Sushko, P. V., Hashimoto, Y., Shluger, A. L. & Hosono, H. Hydride ions in oxide hosts hidden by hydroxide ions. *Nat. Commun.* **5**, 3515 (2014).
27. Hayashi, K., Hirano, M. & Hosono, H. Thermodynamics and Kinetics of Hydroxide Ion Formation in  $12\text{CaO}\cdot 7\text{Al}_2\text{O}_3$ . *J. Phys. Chem. B* **109**, 11900–11906 (2005).
28. Brown, I. D. & Altermatt, D. Bond-valence parameters obtained from a systematic analysis of the Inorganic Crystal Structure Database. *Acta Crystallogr. B* **41**, 244–247 (1985).
29. Ferraris, G. & Ivaldi, G. Bond valence vs bond length in O...O hydrogen bonds. *Acta Crystallogr. B* **44**, 341–344 (1988).
30. Libowitzky, E. Correlation of O-H stretching frequencies and O-H...O hydrogen bond lengths in minerals. *Monatshefte Für Chem. Chem. Mon.* **130**, 1047–1059 (1999).
31. Nakamoto, K., Margoshes, M. & Rundle, R. E. Stretching Frequencies as a Function of Distances in Hydrogen Bonds. *J. Am. Chem. Soc.* **77**, 6480–6486 (1955).
32. Sun, J., Song, C., Ning, S., Lin, S. & Li, Q. Preparation and Characterization of Storage and Emission Functional Material of Chlorine Anion:  $[\text{Ca}_{24}\text{Al}_{28}\text{O}_{64}]^{4+}(\text{Cl}^-)_{3.80}(\text{O}^{2-})_{0.10}$ . *Chin. J. Chem. Phys.* **22**, 417 (2009).
33. Tolkacheva, A. S. *et al.* Synthesis of dense ceramics of single-phase mayenite ( $\text{Ca}_{12}\text{Al}_{14}\text{O}_{32}$ )O. *Russ. J. Appl. Chem.* **84**, 907–911 (2011).
34. Rossman, G. R. & Aines, R. D. The hydrous components in garnets: Grossular-hydrogrossular. *Am. Mineral.* **76**, 1153–1164 (1991).
35. Kolesov, B. A. & Geiger, C. A. The vibrational spectrum of synthetic hydrogrossular (katoite)  $\text{Ca}_3\text{Al}_2(\text{O}_4\text{H}_4)_3$ : A low-temperature IR and Raman spectroscopic study. *Am. Mineral.* **90**, 1335–1341 (2015).
36. Hayashi, K. *et al.* Solid State Syntheses of  $12\text{SrO}\cdot 7\text{Al}_2\text{O}_3$  and Formation of High Density Oxygen Radical Anions,  $\text{O}^-$  and  $\text{O}^{2-}$ . *Chem. Mater.* **20**, 5987–5996 (2008).
37. Cohen-Addad, C., Ducros, P. & Bertaut, E. F. Etude de la substitution du groupement  $\text{SiO}_4$  par  $(\text{OH})_4$  dans les composés  $\text{Al}_2\text{Ca}_3(\text{OH})_{12}$  et  $\text{Al}_2\text{Ca}_3(\text{SiO}_4)_{2.16}(\text{OH})_{3.36}$  de type grenat. *Acta Crystallogr.* **23**, 220–230 (1967).
38. Lager, G. A., Armbruster, T. & Faber, J. Neutron and X-ray diffraction study of hydrogarnet  $\text{Ca}_3\text{Al}_2(\text{O}_4\text{H}_4)_3$ . *Am. Mineral.* **72**, 756–765 (1987).
39. Lager, G. A., Armbruster, T., Rotella, F. J. & Rossman, G. R. OH substitution in garnets: X-ray and neutron diffraction, infrared, and geometric-modeling studies. *Am. Mineral.* **74**, 840–851 (1989).
40. Armbruster, T. Structure refinement of hydrous andradite,  $\text{Ca}_3\text{Fe}_{1.54}\text{Mn}_{0.20}\text{Al}_{0.26}(\text{SiO}_4)_{1.65}(\text{O}_4\text{H}_4)_{1.35}$ , from the Wessels mine, Kalahari manganese field, South Africa. *Eur. J. Mineral.* 1221–1226, doi:10.1127/ejm/7/5/1221 (1995).
41. Sacerdoti, M. & Passaglia, E. The crystal structure of katoite and implications within the hydrogrossular group of minerals. *Bull. Minéralogie* 1–8 (1985).
42. Galuskina, I. O., Galuskin, E. V. & Sitarz, M. Atoll hydrogarnets and mechanism of the formation of achtarandite pseudomorphs 49–62. *Neues Jahrb. Mineral. Monatshefte* 49–62 (1998).
43. Kajihara, K., Matsuishi, S., Hayashi, K., Hirano, M. & Hosono, H. Vibrational Dynamics and Oxygen Diffusion in a Nanoporous Oxide Ion Conductor  $12\text{CaO}\cdot 7\text{Al}_2\text{O}_3$  Studied by  $^{18}\text{O}$  Labeling and Micro-Raman Spectroscopy. *J. Phys. Chem. C* **111**, 14855–14861 (2007).
44. Amthauer, G. & Rossman, G. R. The hydrous component in andradite garnet. *Am. Mineral.* **83**, 835–840 (2015).
45. Andrut, M., Wildner, M. & Beran, A. The crystal chemistry of birefringent natural uvarovites. Part IV. OH defect incorporation mechanisms in non-cubic garnets derived from polarized IR spectroscopy. *Eur. J. Mineral.* 1019–1026, doi:10.1127/0935-1221/2002/0014-1019 (2002).
46. Schröpfer, L. & Bartl, H. Oriented decomposition and reconstruction of hydrogarnet,  $\text{Ca}_3\text{Al}_2(\text{OH})_{12}$ . *Eur. J. Mineral.* 1133–1144, doi:10.1127/ejm/5/6/1133 (1993).
47. Zabinski, W. Studium mineralow grupy hydrogranatu. *AGH W Krakowie Zesz. Nauk.* **38** (1965).
48. Cheng, W., Greenwood, H. J., Hu, H. & Frost, D. C. XRD and XPS analysis of the Grossular-Hydrogrossular series. *Can. Mineral.* **28**, 87–91 (1990).
49. Pytel, Z. Synteza hydrogranatów z szeregu grossular-hydrogrossular w układzie  $\text{C}_3\text{A}\text{-SiO}_2\text{-H}_2\text{O}$  w warunkach hydrotermalnych. *Mater. Ceram. Ceram. Mater.* **65**, 332–342 (2013).
50. Sheldrick, G. M. A short history of SHELX. *Acta Crystallogr. A* **64**, 112–122 (2008).

## Acknowledgements

We would like to thank Thomas Armbruster and Frank Gfeller for factual support during the X-ray data development, discussion, and any comments, Anna Nowak and Maria Czaja for language corrections as well as Radu Bailau for the help in preparation of chlormayenite crystals in order to carry out the temperature measurements. The work was supported by the National Science Centre (NCN) of Poland, grant no. 2013/11/B/ST10/00272.

## Author Contributions

M.D. wrote the text and prepare Figures. E.G. and I.G. wrote the mineralogical part of the text and consult of the problems during the interpretation. J.K. made an XRD measurements and prepare \*.cif files. K.M.M. and K.M. carried out Raman measurements and help during data interpretation.

## Additional Information

**Supplementary information** accompanies this paper at doi:10.1038/s41598-017-08152-1

**Competing Interests:** The authors declare that they have no competing interests.

**Publisher's note:** Springer Nature remains neutral with regard to jurisdictional claims in published maps and institutional affiliations.



**Open Access** This article is licensed under a Creative Commons Attribution 4.0 International License, which permits use, sharing, adaptation, distribution and reproduction in any medium or format, as long as you give appropriate credit to the original author(s) and the source, provide a link to the Creative Commons license, and indicate if changes were made. The images or other third party material in this article are included in the article's Creative Commons license, unless indicated otherwise in a credit line to the material. If material is not included in the article's Creative Commons license and your intended use is not permitted by statutory regulation or exceeds the permitted use, you will need to obtain permission directly from the copyright holder. To view a copy of this license, visit <http://creativecommons.org/licenses/by/4.0/>.